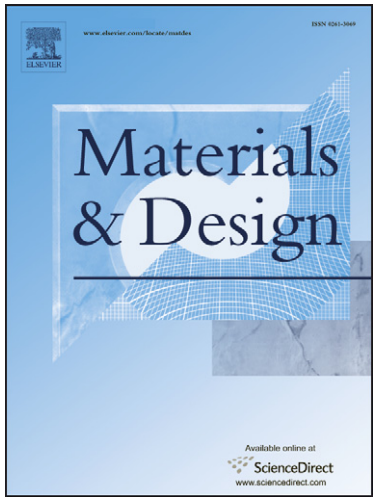

Microstructure and Mechanical Properties of Large Size As-cast Ti-43Al-9V-0.2Y (at.%) Alloy Ingot from Brim to Centre

Fantao Kong, Xingchen Xu, Yuyong Chen, Deliang Zhang

PII: S0261-3069(11)00322-0
DOI: 10.1016/j.matdes.2011.04.053
Reference: JMAD 3775

To appear in: *Materials and Design*

Received Date: 11 February 2011
Accepted Date: 26 April 2011

Please cite this article as: Kong, F., Xu, X., Chen, Y., Zhang, D., Microstructure and Mechanical Properties of Large Size As-cast Ti-43Al-9V-0.2Y (at.%) Alloy Ingot from Brim to Centre, *Materials and Design* (2011), doi: 10.1016/j.matdes.2011.04.053

Microstructure and Mechanical Properties of Large Size As-cast Ti-43Al-9V-0.2Y (at.%) Alloy Ingot from Brim to Centre

Fantao Kong[a,c,*], Xingchen Xu[a], Yuyong Chen[a], Deliang Zhang[b]

[a]*School of Materials Science and Engineering, Harbin Institute of Technology, Harbin 150001, P.R.China*

[b]*Waikato Centre for Advanced Materials, School of Engineering, The University of Waikato, Private Bag 3105, Hamilton, New Zealand*

[c]*State Key Laboratory of Advanced Welding Production Technology, Harbin 150001, P.R.China*

* Corresponding author, Email: kft@hit.edu.cn (Fantao Kong)

Tel: +86 451 86418802, Fax: +86 451 86418802

Microstructure and Mechanical Properties of Large Size As-cast Ti-43Al-9V-0.2Y (at.%) Alloy Ingot from Brim to Centre

Fantao Kong[a,c,*], Xingchen Xu[a], Yuyong Chen[a], Deliang Zhang[b]

[a]*School of Materials Science and Engineering, Harbin Institute of Technology, Harbin 150001, P.R.China*

[b]*Waikato Centre for Advanced Materials, School of Engineering, The University of Waikato, Private Bag 3105, Hamilton, New Zealand*

[c]*State Key Laboratory of Advanced Welding Production Technology, Harbin 150001, P.R.China*

Abstract: A Ti-43Al-9V-0.2Y (at.%) alloy ingot with the size of Φ160×400mm was prepared by vacuum arc remelting (VAR). The microstructure of the as-cast Ti-43Al-9V-0.2Y alloy was composed of B2/α_2/γ lamellar colonies and massive B2 and γ phases which were distributed along the boundaries of these lamellar colonies in the form of equiaxed grains. Based on the grain size variation along the radius direction of the ingot, the ingot could be divided into four ring regions from brim to centre. It has been understood that the grain size variation between these four regions was due to the interplay of the effects of the cooling rate and the yttrium content on solidified microstructures in these regions. Mechanical testing of the samples cut from these four regions showed that there existed a clear correlation between the yield strength and the average grain sizes of the four ring regions, which approximately conformed to a Hall-Petch relationship.

Keywords: A. Intermetallics; C. Casting; F. Microstructure

1. Introduction

TiAl based alloys are promising materials for aerospace applications and automotive engine components due to their low density, high elastic modulus, excellent oxidation resistant and good high temperature mechanical properties [1,2]. Among the hot forming methods of the TiAl based alloys, ingot metallurgy method is an attractive route because of the high mechanical properties and fine grain sizes of the final products [3,4]. Since the hot processing properties of TiAl based alloys depend strongly on their chemical constituents and microstructures, the microstructure control and alloy design have been widely studied to enable optimization of the processing ability of TiAl based alloys in recent years [5,6]. However, TiAl based alloys still generally exhibit limited hot workability at elevated temperatures, which restricts them from being widely used for many desirable applications [7].

To improve the hot workability of as-cast TiAl based alloy ingots, two main methods have been used in previous studies. The first method was to improve the composition homogeneity of as-cast TiAl based alloys [3,7]. The second method was to control solidified microstructure [8,9]. High homogeneity in alloy chemical composition and fine solidified microstructure of the as-cast ingots are helpful to improve their hot workability. Grain refinement of the as-cast alloy ingots was often achieved through adding alloying elements such as C [10], B [11] and Y [12]. In addition, the grain refinement could also be achieved by increasing the volume fraction of β phase in the as-cast microstructure through adding β phase stabilizing elements, such as V, Mo, Cr, Mn and Fe [6,8]. So far, most of the investigations on the effect of adding high contents β stabilizing alloying elements have been performed on small ingot samples [13,14]. The microstructures and mechanical properties of large size ingots produced for practical engineering applications may be different from

those of small ingot samples produced for laboratory based experiments due to the nonuniformity of composition and microstructure of large size ingots. Therefore, it is necessary to understand the variation of composition, microstructure and mechanical properties of the materials at different locations of large size TiAl ingots containing β phase stabilizing elements. The knowledge gained from such study is of crucial importance for optimizing the conditions for hot deformation processing such as extrusion, forging and rolling of the large size ingots. In this study, a large size (Φ160×400mm) TiAl based alloy ingot containing β phase stabilizing element V and grain refining element Y was prepared by vacuum arc remelting (VAR), and the microstructures and mechanical properties of this as-cast ingot at different locations from brim to centre were investigated.

2. Experimental Procedure

An ingot with nominal compositions of Ti-43Al-9V-0.2Y (at.%) was prepared by vacuum arc remelting (VAR). The raw materials used for VAR were titanium sponge (>99.7%), high purity aluminum (>99.99%), and Al-V and Al-Y master alloys. The ingot was remelted 4 times in order to improve its chemical homogeneity. The as-cast Ti-43Al-9V-0.2Y alloy ingot had a diameter of 160mm and a height of 400mm. Average chemical composition of the ingot was analyzed by using X-ray florescence (XRF) technique, and is listed in Table 1. The oxygen content of the ingot was determined using LECO oxygen analyzer, indicating the oxygen content was lower than 700 ppm.

The microstructures of the alloy were studied by using optical microscopy (OM), scanning electron microscopy (SEM/EDX), transmission electron microscopy (TEM) and X-ray diffraction (XRD). The polished surface for OM was etched in a modified Kroll's reagent of 10 vol.% HF, 4 vol.% HNO_3 and 86 vol.% H_2O. Specimens for TEM observation were prepared using a standard procedure and an electrolytic jet polisher. The electrolyte used for the jet polishing was a solution of

60% methanol, 35% n-butyl alcohol and 5% perchloric acid. XRD analysis of the alloys was carried out via Cu Kα radiation (λ= 0.154157 nm) and 2θ from 20° to 120°. Vickers microhardness measurements were carried out on as-cast samples using 200 g indentation load and a 20 s loading time. The tensile tests were carried out at room temperature and a strain rate of 5×10^{-4} s^{-1} using plate specimens with gage section dimensions of 15mm×6.0mm×2.0 mm.

3. Results

3.1 Microstructure

XRD analysis revealed that the as-cast Ti-43Al-9V-0.2Y alloy was composed of three phases: γ, α_2 and B2 phases (Fig. 1). Comparing with those common TiAl based alloys such as Ti-48Al-2Cr-2Nb alloy [2], the as-cast Ti-43Al-9V-0.2Y alloy contained a much higher fraction of B2 phase due to the addition of β stabilizer V which could hold off the decomposition of β phase and change the route of phase transformation. In order to examine the microstructures of the as-cast alloy ingot at different locations from brim to centre, a rectangular sample was cut along the transverse cross-section and at the mid-height of the ingot, as shown schematically in Fig. 2. The macrostructure of the sample is shown in Fig. 3, and it shows that the grains in the ingot are equiaxed, and their sizes clearly changed along the radius of the cross-section of the ingot. Based on the variation of the microstructure from the brim to the centre, the sample could be divided into four regions: A, B, C and D. The average grain sizes of Regions A to D were measured to be approximately 120, 350, 100 and 300μm, respectively.

Fig. 4 shows the SEM backscattered electron images of samples cut from the four regions respectively. The SEM examination showed that the Regions A to D overall had a near-lamellar

structure (NL). Moreover, the SEM backscattered electron images showed the microstructure of each region consisted of lamellar colonies composed of grey/black lamellas (such as Area L), grey/black massive blocks (such as Area M) and a small fraction of white particles. The grey/black massive blocks were distributed along the boundaries of the lamellar colonies. The volume fraction of grey lamellas and massive blocks was about 30%-40%. The variation of the lamellar colony sizes was similar to that of average grain sizes from the brim to the centre of the as-cast alloy ingot. As shown in Fig.4, the volume fraction of lamellar colonies changed significantly from Regions A to D, with the volume fraction of lamellar colonies in Region D being the largest, and followed by those in Regions B, A and C. The volume fraction of lamellar colonies in Region C was down to be about 50-60% (Fig. 4(c)), which showed that microstructure in this region was very close to duplex structure (DP).

The compositions of different microstructural features revealed by the SEM examination (Fig. 4) were determined semi-quantitatively by EDX analysis, and the results are shown in Table 2. Based on the results of the EDX analysis, the phases and compositions of the microstructural features as reflected by the color contrast in the SEM backscaterred electron images were as follows:

(1) Most of the black lamella/massive grains were γ phases which had a composition shown in Zone I with the atomic percentages of Ti and Al being similar. SEM examination could not reveal α_2 phases in the microstructure due to their small size. By TEM examination, a very small amount of α_2 phase plates were observed in the black lamellas, as shown in Fig. 5.

(2) The grey lamella/massive grains were B2 phase which had a composition shown in Zone II with the V content being much higher than that in other phases because V element is the β phase

stabilizer.

(3) The white strips and most of the white particles were YAl_2 phase which had a composition shown in Zone III. This is consistent with the YAl_2 phase observed by authors in Ti-45Al-5Nb-0.3Y alloy [12].

(4) A small amount of little white particles were Y_2O_3 phase which had a composition shown in Zone IV. The formation of Y_2O_3 particles was likely due to the fact that the rare earth element Y was rather active, and tended to react with oxygen in the alloy at high temperatures. The contents of Y_2O_3 and YAl_2 phases in the alloy were too low to be detected by the XRD.

Table 2 also shows the average compositions of each region as determined by the EDX analysis, indicating that the contents of Ti, Al, and V varied very little among the four regions, but the Y content varied remarkably. In Regions A and D, the Y contents were very close to that given in the average chemical composition of the ingot, but the Y content in Region B was lower and the Y content in Region C was much higher than that given in the average composition of the ingot.

Fig. 5 shows typical TEM bright field images of specimens cut from Region D of the as-cast Ti-43Al-9V-Y alloy. As shown in Fig.5(a), the fine structure of the lamella shown in the SEM image (Fig. 4(d)) consisted of irregular and discontinuous lamella of B2 (dark phase in Fig. 5(a)) and γ (grey phase in Fig. 5(a)) phases and a small volume fraction of thin α_2 plates. Along the boundaries of the lamellar colonies, equiaxed γ and B2 grains were also observed, as shown in Fig. 5(b), which was consistent with the observation made in SEM examination as shown in Fig. 4. The TEM examination also showed that the fine structures of the major microstructural features in the other three regions were similar.

3.2 Mechanical Properties

Table 3 shows the room temperature tensile properties and Vickers hardness of samples cut from Regions A, B, C and D, respectively. It was found that the strength, elongation to fracture and hardness of the samples cut from Regions A to D varied significantly, as shown in Table 3. It also appeared that the yield strength and hardness of samples cut from different regions correlated very well with their average grain sizes. In Fig.6, the yield strength ($\sigma_{0.2}$) is plotted as a function of $d^{-1/2}$ for Regions A - D, where d is the average grain size. Based on the data points, a best-fit linear line which showed the dependence of the yield strength on the grain size of the as-cast alloy was plotted and this line can be expressed as follow:

$$\sigma_{0.2} = 386.3 + 1.603 d^{-1/2} \quad (1)$$

The best-fit coefficient of the above linear equation to the experimental data, R^2, is 0.974 which is very high, indicating that there exists a linear correlation between the yield strength and $d^{-1/2}$. This suggests that the as-cast alloy conforms to the Hall-Petch relationship. Alloying elements that led to the formation of fine precipitates in TiAl based alloys might result in the increasing of the values of Hall-Petch constant k_y and σ_0 [15]. Compared with the common TiAl based alloys, such as Ti-47Al alloy (k_y=1.18MPa $m^{-1/2}$, σ_0=221MPa [15]), adding Y in Ti-43Al-9V alloy gave rise to the increasing of the values of k_y and σ_0 (k_y=1.603MPa $m^{-1/2}$, σ_0=386.3MPa), which might be due to the formation of fine precipitates such as YAl_2 and Y_2O_3 particles.

4. Discussion

4.1 Grain size variation

Fig.7 shows a schematic diagram of the structure of the vacuum arc remelting furnace used in

making the ingot. Based on the structure of the furnace, it can be expected that the cooling rate (CR) of the ingot must decrease from the brim to the center during solidification and subsequent cooling, and for a given position in height, the solidification must start from the brim and proceed to the center. In addition, previous research results showed that adding yttrium could clearly refine the grains of TiAl based alloys, and the grain refinement effect increased with increasing the yttrium content [5,12]. This can be explained by the grain growth restriction theory [16], as shown in section 4.2. Therefore, it can be understood from this study that the observed significant and unique grain size variation from the brim to the center of the ingot was due to the combined effects of cooling rate and yttrium content on the solidified microstructure of the ingot. The following is a detailed explanation.

Since the liquid in Region A was in contact with the water cooled copper mould and also away from the centre of arc, the cooling rate of the liquid in this region was very high. This rapid cooling during solidification of the liquid could result in grain refinement of Region A of the as-cast ingot, leading to formation of fine grains as shown in Fig. 4. However, in Region A, the cooling rate and the solidification rate might be so quick that the effect of Y in reducing the grain size was not obvious, and the segregation of Y was very much absent as shown by the observation that yttrium content in this region was very similar to that defined by the average chemical composition of the alloy.

From Fig.4, it was also observed that the grains were much larger in Region B which was next to Region A but further away from the wall of the copper crucible and closer to the centre of the arc than Region A. The larger grains in this region could be attributed to the much lower cooling rate during the solidification in this region than that in Region A. Due to the slower cooling rate and

corresponding solidification rate, the growing solid would have more time to eject Y atoms into the liquid, thus enriching the remaining liquid phase with a higher content of Y than that defined by the average alloy composition. With a similar or slightly lower cooling rate of the liquid, but sufficiently high content of Y in the liquid, the growth of the solid grains was more strongly restricted by the higher Y content, and thus led to formation of more and finer grains than those in Region B, This is Region C as shown in Fig. 4. Since the cooling rate in Region C was similar to that in Region D, but the liquid in Region D was not much enriched with Y due to the longer distance from Region B, as shown by the chemical analysis results presented above, the grain size in Region D became large again.

4.2 The effect of yttrium on grain size

It is expected that the partition coefficient of Y in the solidifying Ti-Al alloy melt must be very low based on the fact that the partition coefficients of Y in the Ti melt is quite low (about 0.09) [17]. This makes Y to be a very effective element for grain refinement according to the grain growth restriction theory [16]. During solidification process, the relative contribution of a solute to the development of constitutional undercooling can be predicted using the growth restriction factor [16]. Approximatively, the grain size, *d*, can be related to alloy content through the growth restriction factor by

$$d = a + \frac{b}{Q} \tag{2}$$

where *a* and *b* are fitted constants, *Q* is the growth restriction factor. Solutes that have a high growth restriction factor will therefore partition strongly ahead of the advancing interface, resulting in the rapid build up of constitutional undercooling [16]. *Q* is generally defined by the following

approximation equation:

$$Q = \sum_i m_i c_{0,i}(k_i - 1) \tag{3}$$

where for each element i, m is the liquidus gradient, c_0 is the composition (wt.%) and k is the binary partition coefficient as calculated from the binary alloy phase diagram. The binary phase diagrams have been used to calculate $m_i(k_i-1)$ values for several solutes in titanium as presented in Table 4 [17].

Therefore, for Ti-43Al-9V-0.2Y alloy, Q and d can be estimated using the following equations:

$$Q = 7.93c_Y \tag{4}$$

$$d = a + \frac{b}{7.93c_Y} \tag{5}$$

where c_Y is the content of yttrium. Equations (4) and (5) suggest that the growth restriction factor increases and the size of β grains formed by solidification of Ti-43Al-9V-0.2Y alloy decreases with increasing the yttrium content. Although YAl_2 intermetallic were observed in the as-cast microstructure, the intermetallic could not refine the prior-β grain size during solidification because the melting point of the intermetallic is much lower than that of prior-β phase. In addition, because the precipitation of Y_2O_3 particles was earlier than that of the prior-β nuclei, Y_2O_3 particles would inhibit the prior-β grain growth. But there were fewer Y_2O_3 particles in the alloy melt (lower oxygen content), the contribution of Y_2O_3 particles for refining the prior-β grain size was significantly less than that of yttrium elements.

5. Conclusions

(1) As-cast Ti-43Al-9V-0.2Y alloy prepared by vacuum arc remelting (VAR) was composed of

B2/α_2/γ lamellar colonies and massive B2 and γ phase which were distributed along the boundaries of these lamellar colonies in the form of equiaxed grains.

(2) The Ti-43Al-9V-Y alloy ingot could be divided into four ring-shaped regions from brim to centre, and the average grain sizes of the four regions (named as Regions A-D) varied from fine to coarse, then to fine again, and then to coarse again. The interesting and unique variation of the grain sizes between these regions could be understood by considering the interplay between the effects of cooling rate and yttrium content in these regions.

(3) Mechanical testing results showed that there existed a clear correlation between the yield strength and the average grain sizes of the four ring regions, which approximately conformed to the Hall-Petch relationship.

Acknowledgements

This work was supported by the National Natural Science Foundation of China under Contract no. 51074058. The authors (Fantao Kong and Deliang Zhang) gratefully acknowledge the funding from the Foundation for Research Science and Technology (FRST), New Zealand, which partially supported research work and writing presented in this paper.

References

[1] R. V. Ramanujan, P. J. Maziasz, C. T. Liu. The thermal stability of the microstructure of γ-based titanium aluminides. Acta Mater. 44 (1996) 2611-2642.

[2] A.Loria Edward. Gamma titanium aluminides as prospective structural materials. Intermetallics. 8 (2000) 1339-1345.

[3] Wu Xinhua. Review of alloy and process development of TiAl alloys. Intermetallics. 14 (2006) 1114-1122.

[4] F.T. Kong, Y.Y. Chen, B.H. Li. Influence of yttrium on the high temperature deformability of TiAl alloys. Mater Sci Eng A. 499 (2009) 53-57.

[5] Baohui Li, Fantao Kong, Yuyong Chen. Effect of Yttrium Addition on Microstructures and Room Temperature Tensile Properties of Ti-47A1 Alloy. J Rare Earths. 24 (2006) 352-356.

[6] F. Appel, M. Oehring, R. Wagner. Novel design concepts for gamma-base titanium aluminide alloys. Intermetallics. 8 (2000) 1283-1312.

[7] Fantao Kong, Baohui Li, Yuyong Chen, Jiecai Han. Essence of room temperature brittleness of TiAl based alloys and improving approaches. J Adv Mat. 39 (2007) 33-40.

[8] M. Takeyama, S. Kobayashi. Physical metallurgy for wrought gamma titanium aluminides: Microstructure control through phase transformations. Intermetallics. 13 (2005) 993-999.

[9] H.F. Chladil, H. Clemens, H. Leitner, A. Bartels, R. Gerling, F.P. Schimansky, S. Kremmer. Phase transformations in high niobium and carbon containing γ-TiAl based alloys. Intermetallics. 14 (2006) 1194-1198.

[10] Limei Cha, Christina Scheu, Helmut Clemens, Harald F. Chladil, Gerhard Dehm, Rainer Gerling, Arno Bartels. Nanometer-scaled lamellar microstructures in Ti-45Al-7.5Nb-(0-0.5)C alloys and their influence on hardness. Intermetallics. 16 (2008) 868-875.

[11] U. Hecht, V. Witusiewicz, A. Drevermann, J. Zollinger. Grain refinement by low boron additions in niobium-rich TiAl-based alloys. Intermetallics. 16 (2008) 969-978.

[12] Yuyong Chen, Baohui Li, Fantao Kong. Microstructural refinement and mechanical properties of Y-bearing TiAl alloys. J Alloys Compd. 457 (2008) 265-269.

[13] T.T.Cheng, M.H.Loretto. The decomposition of the beta phase in Ti-44Al-8Nb and Ti-44Al-4Nb-4Zr-0.2Si alloys. Acta Mater. 46 (1998) 4801-4819.

[14] H. Clemens, H.F. Chladil, W. Wallgram, G.A. Zickler, R. Gerling, K.-D. Liss, S. Kremmer, V.

Güther, W. Smarsly. In and ex situ investigations of the β-phase in a Nb and Mo containing γ-TiAl based alloy. Intermetallics. 16 (2008) 827-833.

[15] Jiancheng Tang, Baiyun Huang, Yuehui He, Wensheng Liu, Kechao Zhou, Aihua Wu. Hall-petch relationship in two phase TiAl alloys with fully lamellar microstructures. Mater Res Bull. 37 (2002) 1315-1321.

[16] M.J. Bermingham, S.D. McDonald, D.H. St John, M.S. Dargusch. Titanium as an endogenous grain-refining nucleus. Philos Mag. 90 (2010) 699-715.

[17] M.J. Bermingham, S.D. McDonald, D.H. StJohn, M.S. Dargusch. Beryllium as a grain refiner in titanium alloys. J Alloys Compd. 481 (2009) 20-23.

Figure captions

Fig.1: XRD pattern of as-cast Ti-43Al-9V-0.2Y alloy.

Fig.2: Schematic diagram showing the orientation, shape and location of the sample taken from the ingot.

Fig.3: Macrostructure of as-cast Ti-43Al-9V-0.2Y alloy.

Fig. 4: SEM backscattered electron images showing the microstructures of as-cast Ti-43Al-9V-0.2Y alloy in different regions: (a) Region A; (b) Region B; (c) Region C; (d) Region D.

Fig. 5: TEM bright field images of a specimen cut from region D of the as-cast Ti-43Al-9V-0.2Y alloy ingot showing (a) a lamellar structure and (b) massive equiaxed grains of B2 and γ phases.

Fig. 6: The yield strength vs $d^{-1/2}$ of the alloy.

Fig. 7: Schematic diagram showing the structure of the vacuum arc remelting furnace and process.

Table captions

Table 1: Average chemical composition of the as-cast Ti-43Al-9V-0.2Y alloy ingot.

Table 2: The compositions of different microstructural features (as divided by the zones I to IV) and regions of the as-cast Ti-43Al-9V-0.2Y alloy ingot, as determined by semi-quantitative composition analysis using EDX (at.%).

Table 3: Room temperature tensile properties of the samples cut from the four regions.

Table 4: Calculated $m_i(k_i-1)$ values for element *i* in titanium [17].

Figures

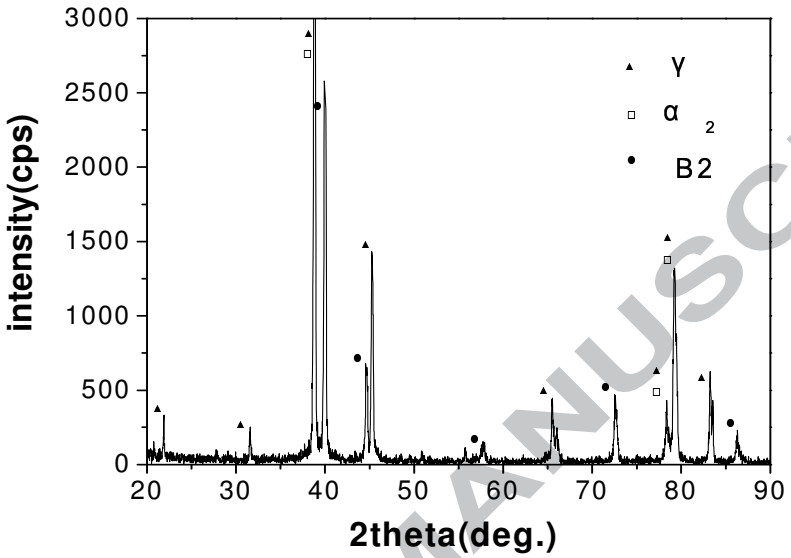

Fig.1: XRD pattern of as-cast Ti-43Al-9V-0.2Y alloy.

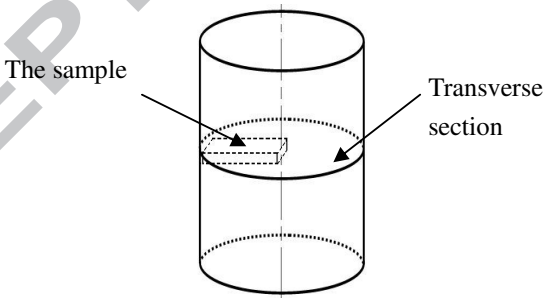

Fig.2: Schematic diagram showing the orientation, shape and location of the sample taken from the ingot.

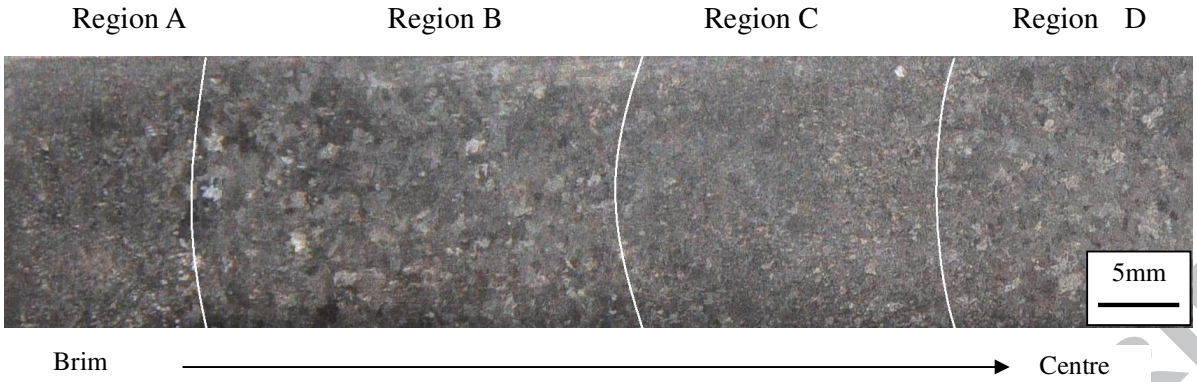

Fig.3: Macrostructure of as-cast Ti-43Al-9V-0.2Y alloy.

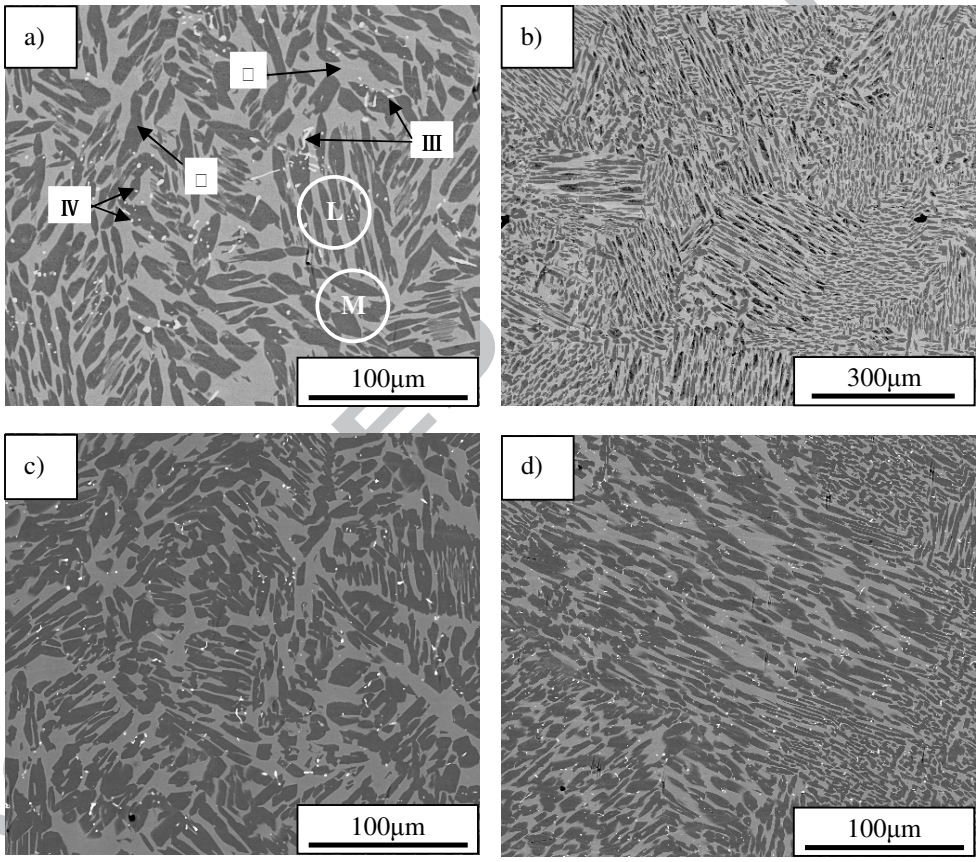

Fig. 4: SEM backscattered electron images showing the microstructures of as-cast Ti-43Al-9V-0.2Y alloy in different regions: (a) Region A; (b) Region B; (c) Region C; (d) Region D.

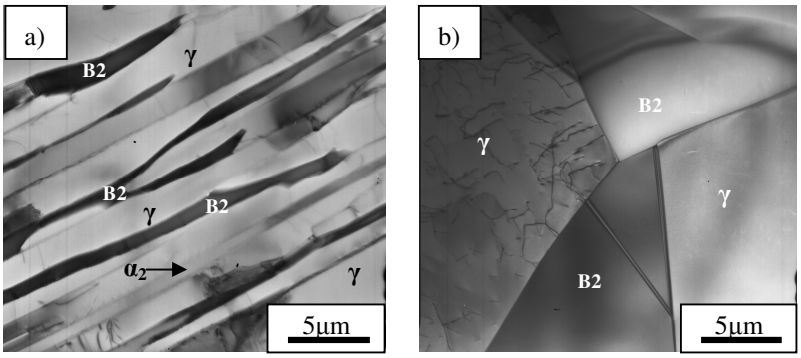

Fig. 5: TEM bright field images of a specimen cut from region D of the as-cast Ti-43Al-9V-0.2Y alloy ingot showing (a) a lamellar structure and (b) massive equiaxed grains of B2 and γ phases.

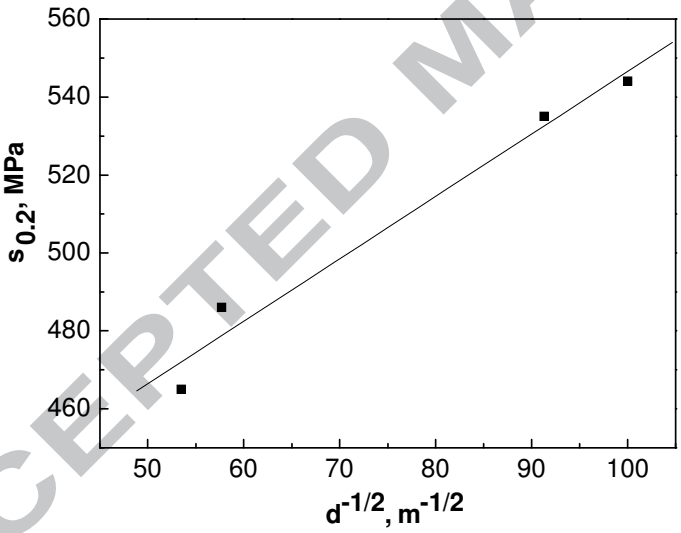

Fig. 6: The yield strength vs $d^{-1/2}$ of the alloy.

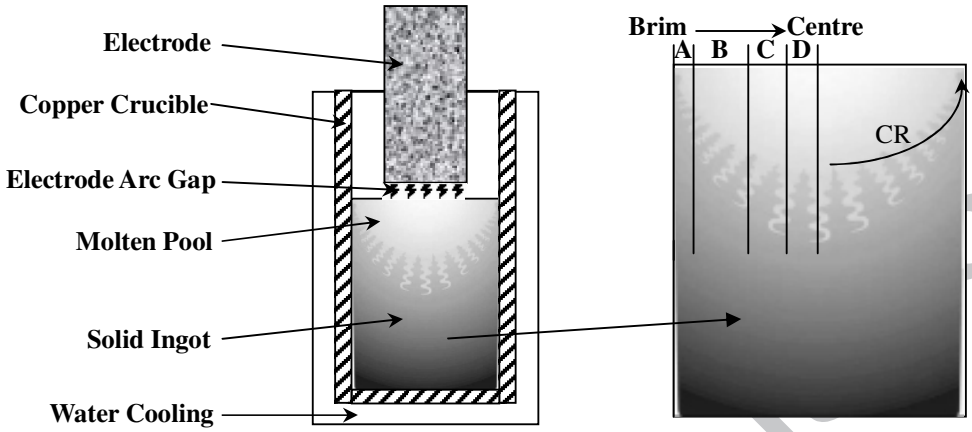

Fig. 7: Schematic diagram showing the structure of the vacuum arc remelting furnace and process.

Tables

Table 1: Average chemical composition of the as-cast Ti-43Al-9V-0.2Y alloy ingot.

Elements	Al	V	Y	Ti
at.%	43.8268	8.7339	0.2283	Bal.

Table 2: The compositions of different microstructural features (as divided by the zones I to IV) and regions of the as-cast Ti-43Al-9V-0.2Y alloy ingot, as determined by semi-quantitative composition analysis using EDX (at.%).

Elements	I	II	III	IV	Region A	Region B	Region C	Region D
Ti	47.17	49.87	9.19	10.81	47.06	48.06	47.03	46.95
Al	48.24	34.93	58.84	7.84	43.96	43.31	43.64	44.01
V	4.59	15.20	2.05	2.53	8.70	8.61	8.85	8.77
Y	-	-	29.92	36.78	0.24	0.17	0.43	0.23
O	-	-	-	42.03	0.04	0.05	0.05	0.04

Table 3: Room temperature tensile properties of the samples cut from the four regions.

Specimen	Grain Size (μm)	σ_b (MPa)	$\sigma_{0.2}$ (MPa)	δ (%)	HV
Region A	120	633.7	534.8	0.71	404
Region B	350	567.8	465.1	0.47	375
Region C	100	614.4	544.2	0.76	403
Region D	300	561.3	486.2	0.45	380

Table 4: Calculated $m_i(k_i-1)$ values for element i in titanium [17].

Element	m_i	k_i	$m_i(k_i-1)$
Al	-2.1	→0	→0
V	-4.7	→0	→0
Y	-8.8	0.09	7.93

Research Highlights

- The microstructures of the TiAl ingot can be divided into four ring-shaped regions from brim to centre.
- The average grain sizes of the four regions vary from fine to coarse, then to fine again, and then to coarse again.
- The growth restriction factor increases and the size of β grains decrease with increasing Y content.